



Functional rGO aerogel as a potential adsorbent for removing hazardous hexavalent chromium: adsorption performance and mechanism

Jingda Chen^{1,2} · Qianwei Liang^{1,2} · Sittipranee Ploychompoo^{1,2} · Hanjin Luo^{1,2,3}

Received: 29 August 2019 / Accepted: 9 December 2019 / Published online: 16 January 2020
© Springer-Verlag GmbH Germany, part of Springer Nature 2020

Abstract

A novel functional rGO aerogel was synthesized by a facile hydrothermal method. In this process, graphene oxide (GO) was used as the precursor and oxidant to synthesize the aerogels. Ethylenediaminetetraacetic acid disodium salt (EDTA-2Na) and pyrrole monomer (reducing agent) were selected to use as hole scavenger and nitrogen sources. The obtained EDTA-2Na/polypyrrole (Ppy)/rGO aerogel (EPGA) has a high adsorption capacity for Cr(VI) anions, and the maximum adsorption capacity reached 361 mg/g at 298 K at pH of 2. In addition, EPGA exhibited a good ability to selectively remove Cr(VI) anions under the effect of coexisting ions (Cl^- , NO_3^- , SO_4^{2-} , PO_4^{3-} , Ni^+ , Cu^{2+} , Zn^{2+} , and Cd^{2+}) and good regeneration ability. The kinetics process and adsorption isotherm can be fitted well with the pseudo-second-order kinetic model and Freundlich isotherm model, respectively. The removal mechanism involved electrostatic interaction, reduction, ion exchange, and chelation process. This work provides a simple and environmentally friendly synthetic route for EPGA, which will be a potential candidate for efficient removal Cr(VI) anions from industrial wastewater.

Keywords Aerogel · Cr(VI) · Adsorption · Reduction

Introduction

In the process of industrial production, a great deal of hexavalent chromium (Cr(VI)) will be discharged, such as semiconductor industry (Aoudj et al. 2015), leather tanneries, electroplating processes and dyes (Jobby et al. 2018). Cr(VI)

pollution is a great threat for human being and ecosystem, because it has high biological toxicity, carcinogenic, and non-biodegradability (He and Chen 2014). Excessive intake of Cr(VI) in the human body can cause a series of diseases, including liver damage, pulmonary congestion, vomiting, and so on (Fang et al. 2007). Therefore, the Environmental Protection Agency lists Cr(VI) as one of the priority pollutants (Geng et al. 2019), and we should attach great importance to the removal of Cr(VI). Currently, methods for removing Cr(VI) from an aqueous solution include photocatalysis, membrane separation, ion exchange, and adsorption, etc. (Han et al. 2019; Liu et al. 2009; Upadhyay et al. 2019). Among these methods, adsorption is considered as the most practical approach due to its high efficiency, economics, and environmentally friendly. Conventional materials, such as activated carbon (Gong et al. 2018), chitosan (Shen et al. 2013), and biochar (Han et al. 2016), have been reported as good adsorbents for the removal of Cr(VI). However, with the Cr(VI) pollution becoming more and more serious, the adsorption capacity of traditional materials is still insufficient, so it is necessary to develop innovative materials to remove Cr(VI).

Responsible Editor: Philipp Gariguess

Electronic supplementary material The online version of this article (<https://doi.org/10.1007/s11356-019-07365-3>) contains supplementary material, which is available to authorized users.

✉ Hanjin Luo
luohj@scut.edu.cn

¹ School of Environment and Energy, South China University of Technology, Guangzhou 510006, People's Republic of China

² The Key Laboratory of Pollution Control and Ecosystem Restoration in Industry Clusters of Ministry of Education, Guangzhou 510006, People's Republic of China

³ Guangdong Engineering and Technology Research Center for Environmental Nanomaterials, Guangzhou 510006, People's Republic of China

Graphene is a new two-dimensional (2D) carbon material with a single-layer structure. It has many excellent properties, such as huge surface area, multiple oxygen functional groups, good electron transfer ability, and superior chemical stability (Chen et al. 2017; Liu et al. 2015). However, under the influence of the strong π - π interaction between graphene sheets and van der Waals force, graphene flakes tend to restack to form graphite-like powders, so that the specific surface area of graphene is much lower than the theoretical value ($2630 \text{ m}^2/\text{g}$) (Cao et al. 2014; Xu et al. 2015). To produce the best possible results of graphene, the suitable approach is making 2D graphene sheets into hierarchical three-dimensional (3D) structure, which retains high specific surface area (Khan et al. 2018; Wan et al. 2016). Besides, the adsorption ability of graphene composites to heavy metal is higher than graphene materials (GO, rGO) (Chen et al. 2015; Li et al. 2018; Najafi et al. 2015; Yang et al. 2010). As we all know that ethylenediaminetetraacetic acid disodium salt (EDTA-2Na) is a common complexing agent in chemistry. It has six coordinating atoms and is capable of forming stable chelates with metal ions. Previous reports showed that EDTA-2Na modified graphene oxide/chitosan composite can improve the removal capacity of Cr(VI), and this composite reached the maximum adsorption capacity (86.2 mg/g) at pH 2 (Zhang et al. 2016). Chauque et al. modified polyacrylonitrile nanofibers with EDTA and the obtained composites had good adsorption capacity for Cr(VI) (66.24 mg/g) (Chauque et al. 2016).

The toxicity of Cr(VI) is almost 100 times that of Cr(III) because the Cr(III) complex is difficult to pass through the cell membrane. Therefore, the conversion of Cr(VI) to Cr(III) is a desirable method for detoxification of Cr(VI) (Jobby et al. 2018). Polypyrrole (Ppy), a conducting polymer, has been widely used in the fields of electrocatalysis, chemical and super capacitors, because it has many unique properties, including facile synthesis, environmental stability, and excellent electrical conductivity (Tuo et al. 2018; Zhang et al. 2018a). More interesting, there are positively charged nitrogen atoms in the polymer chain, so that it can adsorb and reduce Cr(VI) (Bhaumik et al. 2011), which making it possible to extend the application of this conducting polymer to remove Cr(VI). However, Ppy particles have the trend to self-aggregate, owing to its strong π - π interactions, which will reduce specific surface area and hinder its development in Cr(VI) removal (Amalraj et al. 2016). In order to solve this shortcoming, researchers have synthesized Ppy composites, such as modification and copolymerization (Huang et al. 2014). Kera et al. used 2,5-diaminobenzene sulfonic acid to modify Ppy. The composites can selectively remove Cr(VI), with the maximum adsorption capacity of 303 mg/g at 25°C (Kera et al. 2016). Thao et al. synthesized polypyrrole/polyaniline copolymer by interfacial polymerization at the vapor/liquid interface, and FeCl_3 was employed as an oxidant. The adsorption capacity

of the obtained composite material for Cr(VI) was 256.41 mg/g (Thao et al. 2019). Moreover, the polypyrrole can be effectively dispersed through rGO aerogel support, and the performance of Cr(VI) removal can be improved with effect (Zhang et al. 2018a).

Hence, a kind of functional rGO aerogel was successfully synthesized via a hydrothermal self-assembly method in this study. In the preparation process, GO was used as an oxidant to promote the polymerization of pyrrole to form polypyrrole. Ppy and EDTA-2Na were used as cross-linkers and hole scavengers. In addition, they can bring more reactive functional groups to the aerogel. The as-prepared adsorbents were characterized by various methods, such as SEM, XRD, Raman, XPS, and FTIR. In order to better exert the removal effect of the obtained adsorbent on Cr(VI), the effects of initial pH and coexisting ions were investigated. Besides, the reusability and adsorption mechanisms were also investigated.

Materials and methods

Chemicals

Graphite powder was offered by Qingdao Nanshu Ruiying Graphite Co. Ltd. (Qingdao, China). Ethylenediaminetetraacetic acid disodium salt (EDTA-2Na) was purchased from Macklin Reagent Co. Ltd. (Shanghai, China). Pyrrole was obtained from Aladdin Reagent Co. Ltd. (Shanghai, China). Potassium dichromate ($\text{K}_2\text{Cr}_2\text{O}_7$) was of G.R. grade from Sinopharm Chemical Reagent Co. Ltd. (Shanghai, China), while all the other reagents were of analytical grade and used without further purification. All solutions were prepared using deionized (DI) water.

Preparation of EDTA-2Na/Ppy/rGO composite

Graphene oxide (GO) was synthesized by a modified Hummers method (Liang et al. 2018). EDTA-2Na/Ppy/rGO aerogel (EPGA) was synthesized according to a one-step method (Jiang et al. 2016; Zhang et al. 2018b). Briefly, the GO was ultrasonically dispersed in deionized water (1 mg/ml , 30 ml) for 30 min and then certain amount of fresh pyrrole (mass ratio of GO/pyrrole 1:1.5) was added into the above GO dispersion and sonicated for 30 min. Finally, EDTA-2Na (mass ratio of GO/EDTA-2Na 1:5) was added to the solution and sonicated for another 30 min. Then adjust the pH of the mixture to 4 and the mixture was sealed and transferred into a Teflon stainless steel autoclave and heated at 180°C for 6 h. After cooling to the room temperature naturally, the hydrogel was taken out and washed several times with deionized water. Thereafter, the pure hydrogel was freeze dried for 48 h to obtain the aerogel (Fig. 1). Methods for the synthesis of contrast materials, such as GO aerogel (GA), Ppy/GO aerogel

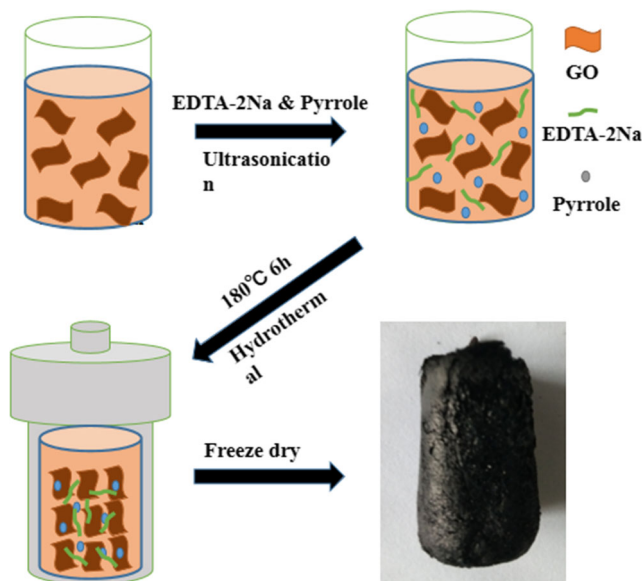


Fig. 1 Schematic of synthesis route of EPGA

(PGA), and EDTA-2Na/GO aerogel (EGA), are displayed in Text. S1.

Apparatus and measurements

The concentration of Cr(VI) (Ministry of Ecology and Environmental of the People’s Republic of China, n.d.-a. GB 7467-87) and total Cr (Ministry of Ecology and Environmental of the People’s Republic of China, n.d.-b, GB 7466-87) were measured by UV-vis spectrophotometer (UV-1750, SHIMADZU, Japan). Scanning electron microscope (SEM, S-3700 N, Hitachi, Japan) was applied to observe the morphology at different magnifications. The X-ray diffraction (XRD) patterns were obtained by a D8-advance X-ray diffractometer (Bruker, Germany) with a Cu K α radiation source ($\lambda = 1.5418 \text{ \AA}$) at a scan rate of $5^\circ/\text{min}$ (2θ range from 5° to 80°), used to understand the crystal structures of the materials. X-ray photoelectron spectroscopy (XPS) analysis was carried on the spectrometer (Thermo Fisher Scientific K-Alpha) with an Al monochromatic X-ray source (1486.6 eV). Fourier transform infrared spectrum (FTIR) were obtained by using a Nicolet-460 (Thermo Nicolet, USA) FTIR spectrophotometer in the range of $500\text{--}4000 \text{ cm}^{-1}$ with a spectral resolution of 4 cm^{-1} . Raman spectrum were carried out on a JYHR800 (France) spectrometer with a wavenumber ranging from 800 to 2000 cm^{-1} .

Batch experiments

The batch adsorption experiments were carried out in a constant temperature shaker at an agitation speed of 200 rpm at $25 \text{ }^\circ\text{C}$. A certain amount of adsorbent (dosage 0.4 mg/ml) was added into Cr(VI) solution ($10\text{--}500 \text{ mg/L}$) under shaken for a

certain time. The pH of solution ranged from 1 to 8, adjusted by 0.1 M HCl and NaOH solution. Kinetics study was carried out at various concentrations of Cr(VI) solution (50 mg/L , 75 mg/L , and 100 mg/L), and the adsorption isotherm experiments were conducted at $25 \text{ }^\circ\text{C}$, $35 \text{ }^\circ\text{C}$, and $45 \text{ }^\circ\text{C}$. The ions (Ni^+ , Cu^{2+} , Zn^{2+} , Cd^{2+} , Cl^- , NO_3^- , SO_4^{2-} , PO_4^{3-}) with the same concentration as Cr(VI) (100 mg/L) were used to study the effect of coexisting ions on Cr(VI) adsorption. After adsorption equilibrium, a $0.45\text{-}\mu\text{m}$ filter membrane was used to separate the adsorbent, and the Cr(VI) concentration in the solution was measured by a UV-vis spectrophotometer. To investigate the regeneration capacity, the EPGA after adsorption of Cr(VI) was desorbed in a 1.0 M NaOH solution and recycled four times. The following equation can be used to calculate the adsorption capacity (q_e , mg/g). All experiments were repeated three times, and the data presented were average.

$$q_e = \frac{(C_0 - C_e)V}{m} \tag{1}$$

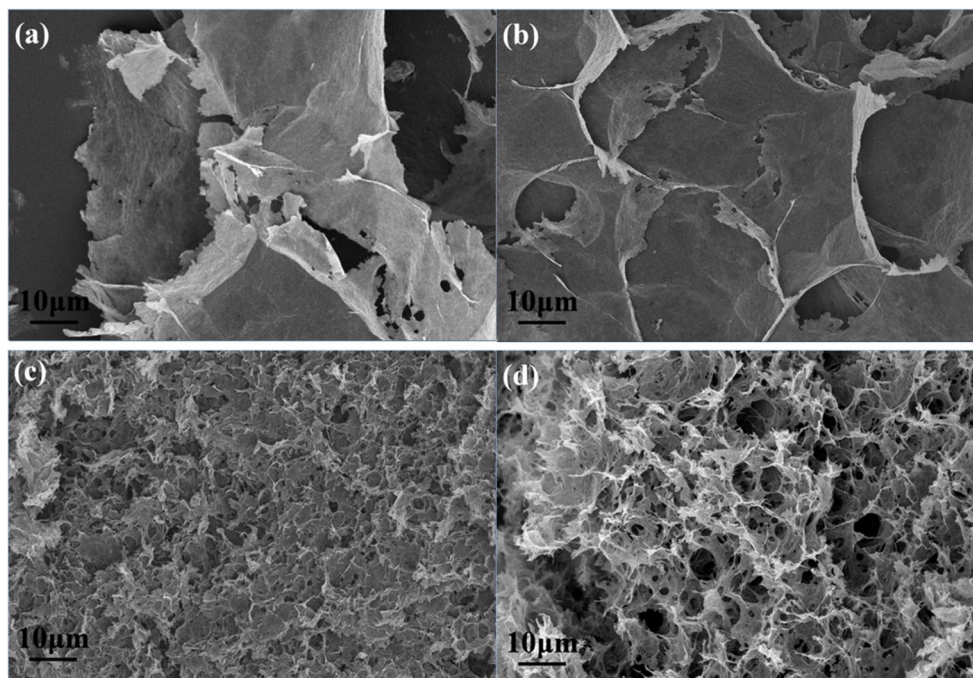
where C_0 and C_e (mg/L) are the initial and equilibrium Cr(VI) concentrations in solution, V (L) is the volume of solution, and m (g) is the adsorbent mass.

Results and discussion

Characterization and analysis

To further investigate the micromorphology, SEM was used to analyze the porous structure and morphologies of GA, PGA, EGA, and EPGA. The morphologies of GA, PGA, EGA, and EPGA were magnified 1000 times; as presented in Fig. 2, GA, PGA, EGA, and EPGA display 3D structures. GA and PGA exhibited nanosheets cross-linked structures, and in the case of introducing the hole scavenger EDTA-2Na, EGA and EPGA showed homogeneous 3D network structure. Compared to EGA, with the introduction of EDTA-2Na and pyrrole, EPGA has more pore structure and a more uniform 3D network structure. The possible explanation is that pyrrole reacted with both GO and EDTA-2Na to form a larger molecular weight complex, which provides better support for the aerogels. Furthermore, the BET surface area of GA determined by the nitrogen adsorption-desorption isotherm curve was $176.2 \text{ m}^2/\text{g}$, and the specific surface area of PGA was $23.9 \text{ m}^2/\text{g}$, which was smaller than GA. This may be due to the fact that the PPy nanoparticles were anchored to the surface and blocked the porous network, resulting in the decrease of the exposed surface area (Fang et al. 2018). For EGA and EPGA, the measured specific surface areas were $75.7 \text{ m}^2/\text{g}$ and $53.6 \text{ m}^2/\text{g}$, respectively. They were smaller than the specific surface area of GA. However, the average pore diameter

Fig. 2 SEM images of **a** GA, **b** PGA, **c** EGA, and **d** EPGA



of EGA (6.9 nm) and EPGA (7.4 nm) was larger than the average pore diameter of GA (4.3 nm).

Figure 3 a depicts the X-ray diffraction patterns of EPGA, GO, GA, EGA, and PGA. The results showed that the sharp diffraction peak at 8.95° and the calculated d -spacing were about 0.99 nm, which can be attributed to GO. However, the peak of GO disappeared after hydrothermal reaction to form GA, PGA, and EGA, indicating that GO has been reduced by deoxygenation. Compared with GO, there was a broad and gentle diffraction peak at 25° and the calculated d -spacing were 0.37 nm, 0.36 nm, and 0.36 nm for GA, PGA, and EGA, showing that the GO involved in the hydrothermal reaction was converted to rGO. The XRD pattern of EPGA showed a broad and weak diffraction at 16.14° – 33.53° , which suggested the amorphous structure of EPGA. In addition, the diffraction peak of EPGA is much lower than PGA and EGA, so we can conclude that the introduction of polypyrrole and EDTA-2Na overlap each other in diffraction and the combination of polypyrrole and EDTA-2Na with GO is mainly through chemical reaction.

The structure of the nanocomposites was further analyzed by Raman spectrum. According to previous reports, we know that graphene materials have two typical peaks at about 1352 cm^{-1} (D-band) and 1596 cm^{-1} (G-band). The G-band is the result of in-plane stretching vibrations of the sp^2 C–C bond in graphene materials, while the D-band corresponds to the defect structure caused by the destruction of the sp^2 domain or introduction of functional groups (Ding et al. 2017; Mondal et al. 2018). As presented in Fig. 3b, GA, PGA, EGA, and EPGA all have a characteristic peak at 1352 cm^{-1} and another characteristic peak at between 1581 and 1597 cm^{-1} ,

demonstrating that all of these aerogels have graphene structure. Furthermore, the G-band of EPGA appeared at 1581 cm^{-1} , but for GO, it was at 1596 cm^{-1} , indicating partial recovery of the sp^2 domain during the functionalization of aerogels (Mondal et al. 2018). Moreover, EPGA has an intensity ratio I_D/I_G of about 1.04, which is slightly higher than GO (1.00) and GA (1.01), demonstrating that there are a large number of defects in the functionalized EPGA. In summary, the results of the Raman spectrum further indicated that the GO involved in the hydrothermal reaction was converted to rGO.

XPS was employed to analyze the variation of elemental composition, and the functional groups of the materials were characterized (Fig. 3c). GA, PGA, EGA, and EPGA have two peaks appeared at 285 eV and 532 eV, corresponding to C1s and O1s. Compared with GA, there was a new peak appeared at 400 eV in PGA and EGA, corresponding to N1s. In addition, EGA has a peak at 496 eV (Na1s), which was derived from EDTA-2Na. Therefore, polypyrrole and EDTA-2Na were successfully introduced into PGA and EGA, respectively. For EPGA, it has the four peaks as described above and the N1s peak is higher than EGA but lower than PGA. Core-level N1s spectra of PGA, EGA, and EPGA are presented in Fig. 4. Compared to PGA and EGA, EPGA has a new peak at 402.2 eV, attributed to pyrrolic-N-oxide, which clearly declared that polypyrrole and EDTA-2Na were introduced into EPGA and polypyrrole was modified by EDTA-2Na. In summary, EDTA-2Na/Ppy/rGO aerogel (EPGA) have been successfully synthesized through hydrothermal reaction, which can be further confirmed by FTIR spectra.

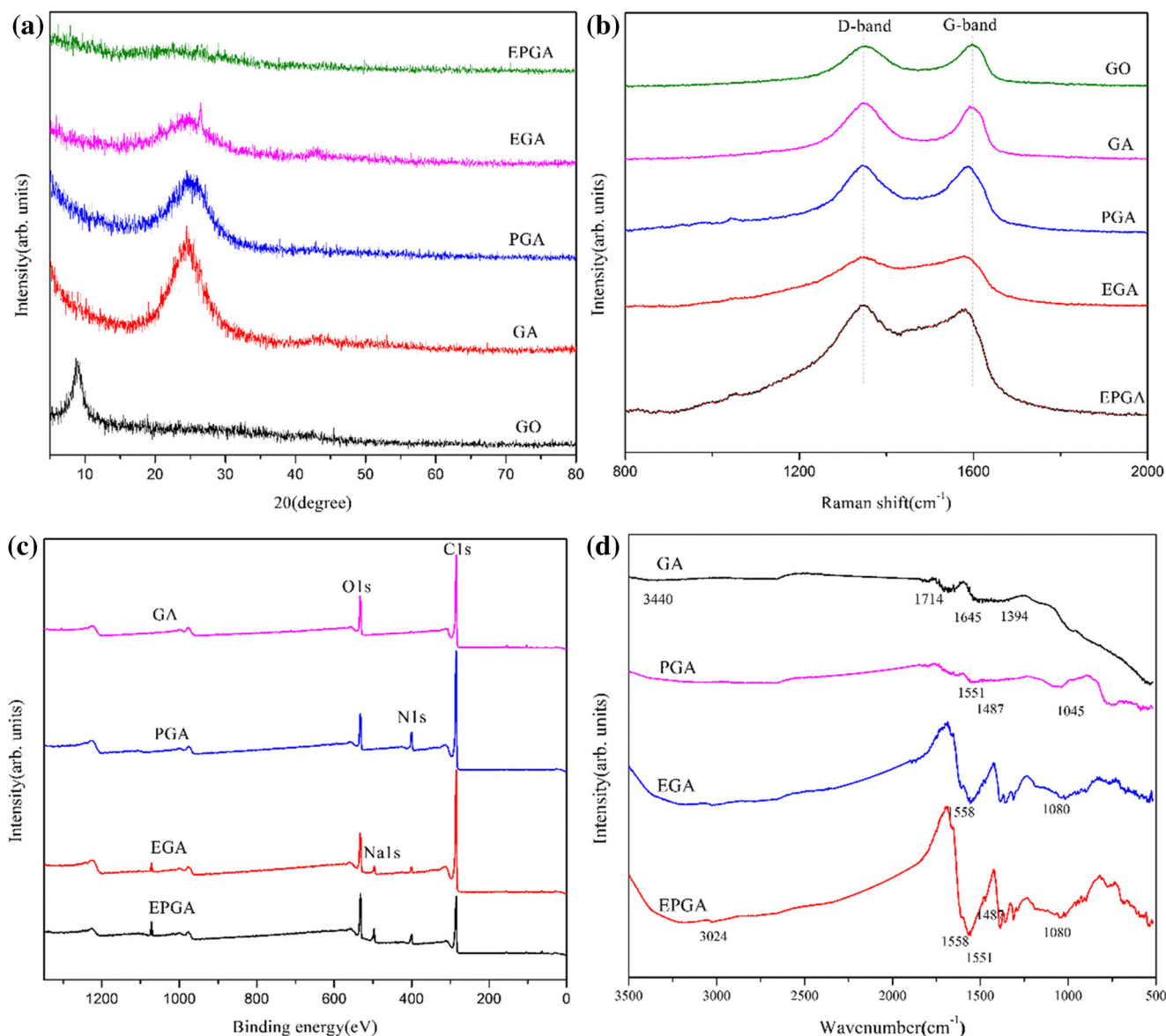


Fig. 3 a X-ray diffraction patterns of GO, GA, PGA, EGA, and EPGA. b Raman spectra of GO, GA, PGA, EGA, and EPGA. c XPS spectra of GA, PGA, EGA, and EPGA. d FTIR spectra of GA, PGA, EGA, and EPGA

FTIR spectroscopy was used to investigate the functional groups of the prepared materials (Fig. 3d and Fig. S1). The peaks of GA appear at 3400, 1714, 1645, and 1394 cm^{-1} , corresponding to the stretching vibration of C–H bonds from the adsorbed H_2O and GO component, C=O stretching vibration of the carboxyl, the stretching vibrations of C=C bonds, and the stretching vibrations of O–H bonds. The main peaks of PGA appeared at 1551 and 1487 cm^{-1} , corresponding to conjugated C–N and C–H stretching vibration from the pyrrole ring (Fang et al. 2018). The band at 1045 cm^{-1} was assigned to N–H in-plane deformation vibration. Compared to PGA, EPGA has new peaks at 1558 and 1080 cm^{-1} , which were caused by the N–H stretching vibration and reflected the introduced EDTA-2Na (Cui et al. 2015). The band at 3024 cm^{-1} can be assigned to the stretching vibrations of C–

H saturated bond. FTIR spectroscopy confirmed that Ppy and EDTA-2Na were introduced into EPGA, which contained a large number of oxygen-containing and nitrogen-containing reactive groups.

Effect of initial pH

Based on previous reports, we can see that pH is one of the most important factor in adsorption of Cr(VI), because pH has a strong impact on the existing state of Cr(VI) anion and protonation of adsorbents. In order to study the effect of pH, the adsorption experiment was carried out in the range of pH from 1 to 8 (dosage 0.4 g/L, concentration 100 mg/L, volume 25 mL). The result is depicted in Fig. 5a. The adsorption capacity of EPGA reached a maximum at pH 2.0 and the

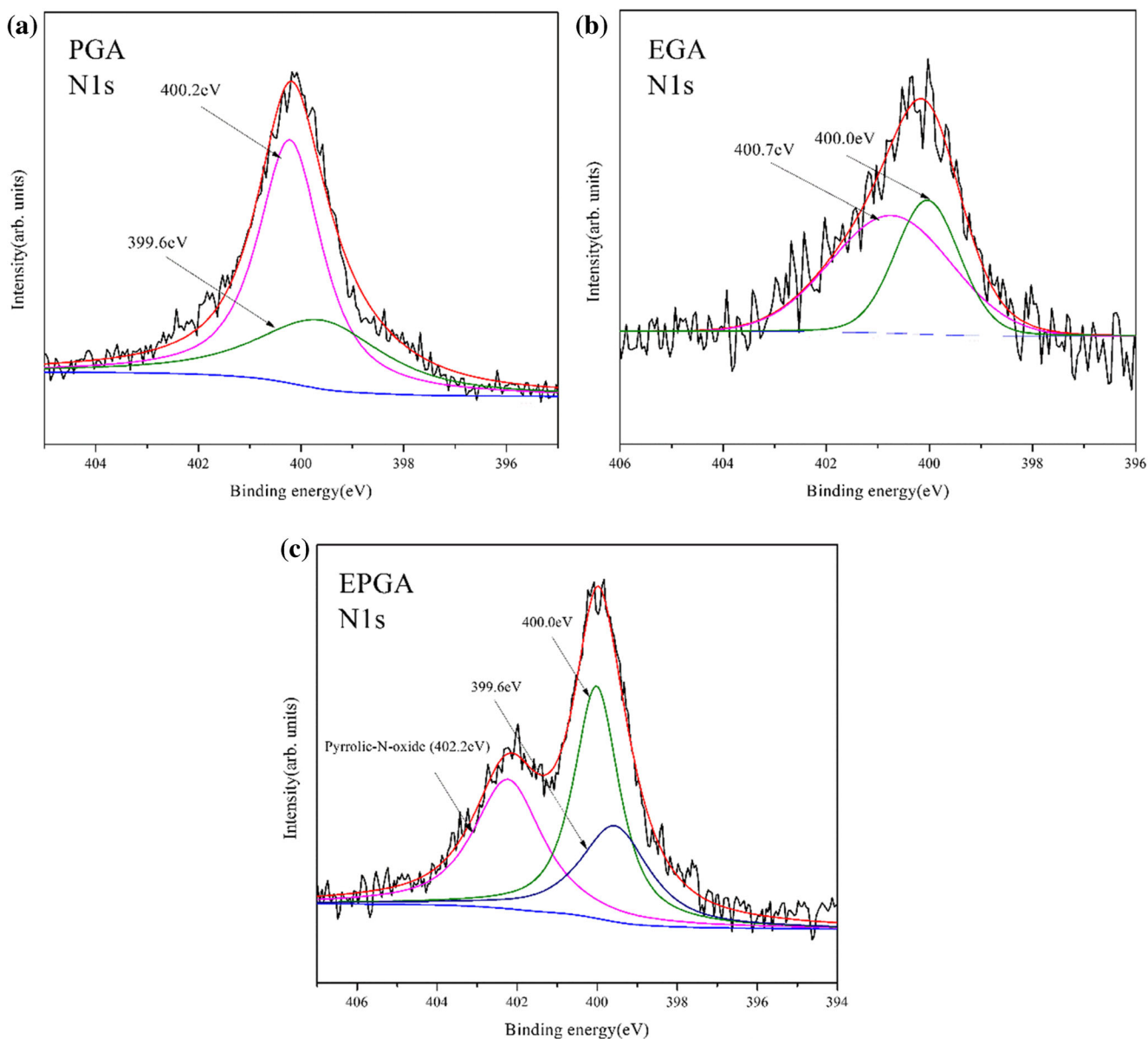


Fig. 4 Core-level N1s spectra of **a** PGA, **b** EGA, and **c** EPGA

adsorption capacity decreased rapidly with the increase of pH. When the pH < 2, the adsorption capacity of EPGA tended to decrease slowly. But the adsorption capacity of EPGA was maintained at a high level at the pH range of 1.0–3.0, which is much higher than other contrast materials (GA, PGA, and EGA). EPGA exhibited excellent adsorption performance at low pH because it has strongest reducing groups, which could partially reduce Cr(VI) to Cr(III). Moreover, it has a large number of reactive groups (–COOH, –NH–) which can be protonated (–COOH⁺, –NH⁺) in acidic conditions, and they could adsorb HCrO₄[–] and Cr₂O₇^{2–} (the dominant species of Cr(VI) at low pH) by electrostatic attraction (Zhang et al. 2016).

The trend of GA, PGA, and EGA adsorption capacity changed similar to EPGA; this phenomenon is related to

adsorbate and adsorbent. Various species of Cr(VI) existed in different pH solutions. Cr₂O₇^{2–} and HCrO₄[–] predominate at acidic pH, while CrO₄^{2–} is dominant at pH > 6. Furthermore, HCrO₄[–] is more readily adsorbed on the surface of the adsorbent than CrO₄^{2–}, because HCrO₄[–] requires only one active site and CrO₄^{2–} requires two active sites (Norouzi et al. 2018). Moreover, surface charge of adsorbent is another important factor. The zeta potential (ζ) was measured at different pH to investigate the surface charge of adsorbents. As shown in Fig. S2, the protonation of the functional groups on the surface of the adsorbent caused the surface charge to be positively charged at low pH, promoting the adsorption of the Cr(VI) anion. As the pH increased, the functional groups on the surface of the adsorbent deprotonated, and the zeta potential decreased. At higher pH, the surface charge of the

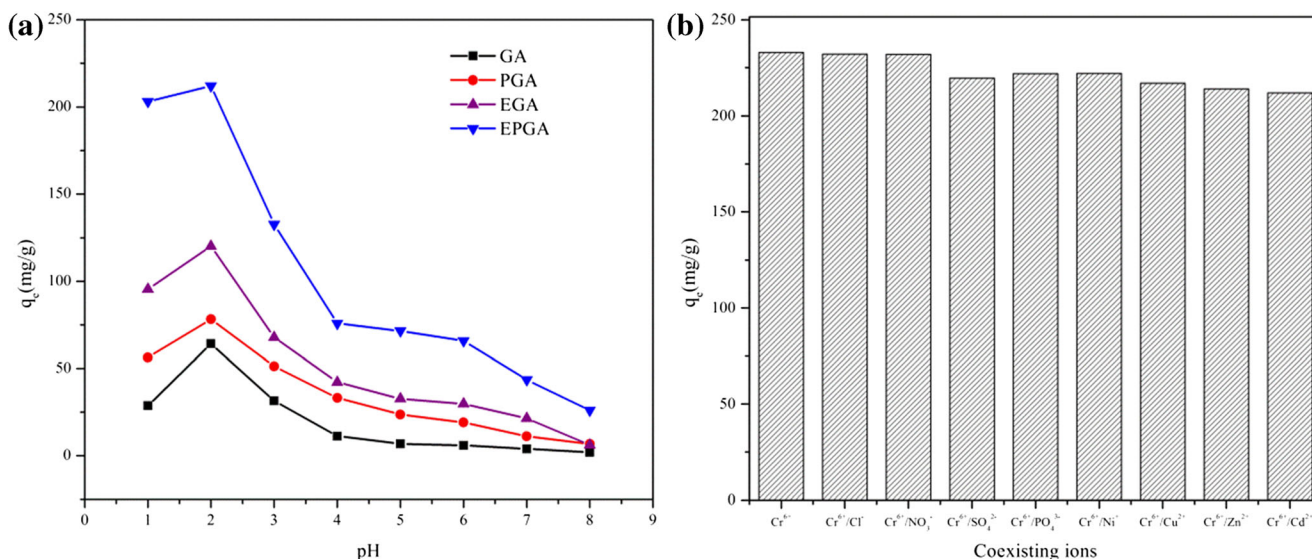


Fig. 5 a Effect of pH on adsorption capacity. b Effect of coexisting ions for adsorption of Cr(VI) onto EGPA

adsorbent was negative, which led to the repulsive force of Cr(VI) adsorption, resulting in a decrease of adsorption capacity.

Effect of coexisting ions

In most cases, the composition of industrial wastewater is complex and may contain one type or more metal cations and a variety of common inorganic anions, such as Cl⁻, NO₃⁻, SO₄²⁻, PO₄³⁻, Cu²⁺, Zn²⁺, Cd²⁺, and Ni⁺. Therefore, it is necessary to study the influence of these coexisting ions in the adsorption process. In the experiment, we kept the concentration of Cr(VI) and coexisting ions in agreement (100 mg/L), and added 10 mg of adsorbent to the solution (dose 0.4 g/L, pH=2, 25 °C). The experimental results are shown in Fig. 5b. We can find that Cl⁻ anions and NO₃⁻ anions have no significant effect on the removal of Cr(VI). However, the other two anions (SO₄²⁻, PO₄³⁻) have an effect on the adsorption of Cr(VI), and the removal efficiency decreased by 5.4 and 4.4%, respectively; owing to SO₄²⁻, PO₄³⁻ anions have similar molecular size and closer ionic radius with HCrO₄⁻ (Cai et al. 2019). Compared with anions, metal cations have a more pronounced effect on the adsorption of Cr(VI) anions. This can be explained as follows: the doping of EDTA-2Na introduced a large number of reactive groups (-COOH) into EPGA, which can complex with most metal ions. In general, coexisting ions have little effect on the adsorption of Cr(VI) by EPGA. Cd²⁺ cations has the greatest influence on the adsorption of Cr(VI), and the removal efficiency was reduced by 8.4%, but still maintains high removal efficiency and large adsorption capacity, indicating that EPGA can selectively remove Cr(VI).

Adsorption kinetics

Excellent adsorbent materials not only need to have high adsorption capacity, but also should be able to achieve adsorption equilibrium in a short time. Kinetics adsorption experiments were performed using three initial Cr(VI) concentrations (50 mg/L, 75 mg/L, 100 mg/L) at different time. The result is shown in Fig. 6. It can be seen that when the initial Cr(VI) concentration was 50 mg/L, the adsorption capacity rapidly increased in the first 80 min and reached the adsorption equilibrium in 180 min. As the initial concentration increased, both the adsorption capacity and the equilibrium time increased (360 min for 75 mg/L, 900 min for 100 mg/L).

To better understand the adsorption mechanism, pseudo-first-order (Eqs. (2)) and pseudo-second-order models (Eqs. (3)) were used to fitting the experimental data.

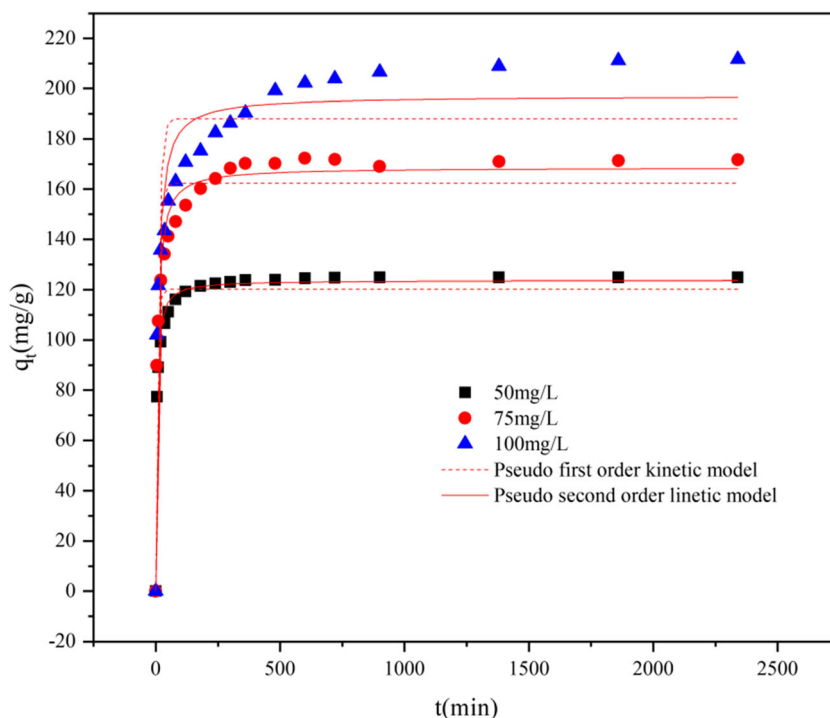
$$q_t = q_e[1 - \exp(-k_1 t)] \tag{2}$$

$$q_t = \frac{q_e^2 k_2 t}{1 + q_e k_2 t} \tag{3}$$

where q_t (mg/g) is the adsorption capacity at time, t ; q_e (mg/g) is the adsorption capacity at equilibrium; k_1 (min⁻¹) and k_2 (g/(mg min)) are the rate constants of the pseudo-first-order model and the pseudo-second-order model, respectively.

The fitting plots of the kinetic data are shown in Fig. 6, and Table 1 shows the kinetic constants and other parameters calculated from the non-linear regression. Since the determination coefficients (r^2) for pseudo-second-order kinetic models are significantly higher than that of pseudo-first-order kinetic model, we can conclude that pseudo-second-order kinetic models fitted the experimental data better for all the concentrations. This suggested that chemisorption between the

Fig. 6 Adsorption kinetics with pseudo-first-order and pseudo-second-order model



EPGA and Cr(VI) was the rate-controlling step (Lyu et al. 2019). Moreover, the calculated adsorption capacity was consistent with the experimental values at various initial concentrations.

Adsorption isotherms

Adsorption isotherms play an important role in the adsorption system, because it can help to understand the distribution of adsorbed molecules between the aqueous and solid phases under equilibrium conditions (Yan et al. 2017). The isothermal adsorption of Cr(VI) on EPGA was studied at 298 K, 308 K, and 318 K, respectively. The result is presented in Fig. 7a; as the equilibrium concentration of Cr(VI) increased, we can see that the adsorption capacity of EPGA increased. This may be due to an increase in driving force at higher concentrations, overcoming the mass transfer resistance of the adsorbate between the aqueous phase and the solid phase (Yuan et al. 2013). Moreover, we could conclude that the adsorption of EPGA was an endothermic process, because the adsorption capacity increased with increasing temperature. More interestingly, at the initial Cr(VI) concentration of 50 mg/L, the Cr(VI) concentration at equilibrium was 4S2 $\mu\text{g/L}$ (Fig. 7b), which indicates that if the initial Cr(VI) concentration is lower than 50 mg/L, the Cr(VI) concentration after adsorption can meet the Chinese industrial wastewater discharge standards (0.5 mg/L) (Ministry of Ecology and Environmental of the People's Republic of China, n.d.-c, GB 8978-96).

Langmuir and Freundlich isotherm models were used to analyze the experimental adsorption data. The Langmuir adsorption model assumes that adsorption is monolayer adsorption. The solid surface is considered to be homogeneous, and each adsorption site has the same affinity for the molecule, resulting in one adsorption site capable of adsorbing only one molecule. The Freundlich isotherm model considers the solid surface to be non-uniform and one molecule can be adsorbed by multiple adjacent binding sites on the solid surface. The adsorption capacity is the sum of adsorption at all sites (Foo and Hameed 2010). The equations were expressed as follows (Liang et al. 2018):

$$q_e = \frac{bq_{max}C_e}{1 + bC_e} \quad (4)$$

$$q_e = k_f C_e^{1/n} \quad (5)$$

where C_e (mg/L) is the Cr(VI) concentration at equilibrium; q_e (mg/g) is the adsorption capacity at equilibrium; q_{max} (mg/g) is the maximum adsorption capacity; b , n and k_f are the Langmuir and Freundlich constants.

The isotherm constants were calculated and summarized in Table 2. The results showed that the determination coefficients (r^2) for Freundlich were higher than that of Langmuir, demonstrating that the Freundlich model fitted the experimental data better. Therefore, the adsorption of Cr(VI) onto EPGA may be multilayer adsorption on the energetically heterogeneous surface. For the Freundlich model, a higher k_f value indicated that EPGA had a higher adsorption capacity and affinity for Cr(VI). The value of n reflects the heterogeneity

Table 1 Comparison of pseudo-first-order and pseudo-second-order kinetic model constants

C_0 (mg/L)	$q_{e,exp}$ (mg/g)	Pseudo-first-order kinetic model			Pseudo-second-order kinetic model		
		K_1 (min ⁻¹)	$q_{e,cal}$ (mg/g)	r^2	K_2 (g/(mg min))	$q_{e,cal}$ (mg/g)	r^2
50	124.91	0.1556	120.3053	0.9429	0.0022	123.8148	0.9912
75	171.69	0.1064	162.3417	0.9074	9.8465×10^{-4}	168.6083	0.9780
100	211.63	0.0913	188.1194	0.8340	6.6048×10^{-4}	197.0520	0.9338

of the adsorbent or the strength of the adsorption reaction and a larger value of n means better adsorption performance. The comparison of adsorption performance of EPGA and other adsorbents on Cr(VI) was shown in Table S1. Compared to these materials, EPGA has excellent adsorption capacity, which indicates that it is a promising adsorbent for removing Cr(VI).

Regeneration performance evaluation

The regenerative properties of the adsorbent reflect its stability to some extent. The stability of the adsorbent plays an important role in the treatment of industrial wastewater, and even affects the development of adsorbent materials. If the adsorbent can be recycled multiple times and still maintain excellent adsorption performance, the economic cost can be reduced. Therefore, the preparation of the adsorbent requires to study its reusability. In order to investigate the reusability of EPGA, we compared the effects of various desorption agents (Fig. S3). And 1 M NaOH solution was selected as the regeneration agent. In Fig. 8, it could be seen that after four times of adsorption-desorption cycle, the adsorption capacity of EPGA decreased from 194 to 143 mg/g, but still

retained 73.7% removal efficiency. It means that EPGA had excellent regeneration ability. Figure 9 d shows that the peak of pyrrolic-N became weak after adsorption. In addition, the FTIR analysis (Fig. S4), showed that the intensity of the peak corresponding to pyrrole was also became weak, but the other peaks did not change significantly after adsorption-desorption. This explained why the removal efficiency after regeneration was slightly decreased, but still maintained high adsorption efficiency.

Adsorption mechanism

In order to investigate the mechanisms of Cr(VI) removal, the EPGA before and after Cr(VI) adsorption were characterized by XPS. The result is shown in Fig. 9a. Compared with the EPGA before loading Cr(VI), a new peak appeared at 577.6 eV in the full-range XPS spectrum of EPGA after Cr(VI) adsorption, which confirmed that Cr was successfully adsorbed onto the surface of EPGA. The Cr2p core-level spectra can be divided into two peaks: Cr2p_{1/2} and Cr2p_{3/2} (Fig. 9b). In addition, both Cr2p_{1/2} and Cr2p_{3/2} were deconvoluted to two components at around 576.8 eV, 578.0 eV, 586.6 eV, and 587.7 eV, which attributed to Cr(III)2p_{1/2}, Cr(VI)2p_{1/2},

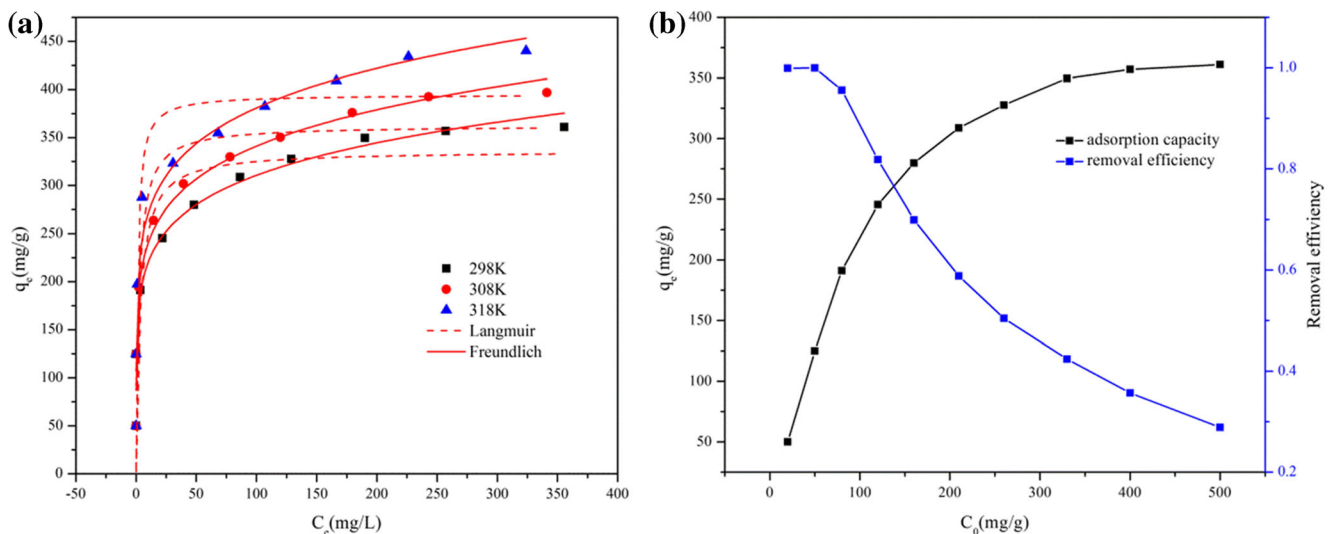


Fig. 7 a Adsorption isotherm. b Removal efficiency at different initial concentrations at pH = 2 at 298 K

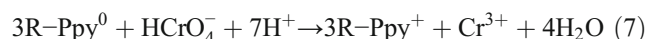
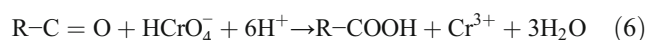
Table 2 Comparison of Langmuir model and Freundlich model constants

Temperature (K)	Langmuir model			Freundlich model		
	q_{max} (mg/g)	b (L/mg)	r^2	k_f	n	r^2
298	336.12695	0.29152	0.75224	156.1177	6.69485	0.97279
308	362.58127	0.40041	0.78873	169.16258	6.56918	0.97686
318	394.84753	0.7935	0.82475	192.76497	6.76208	0.9569

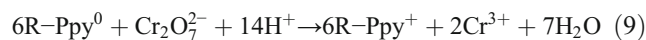
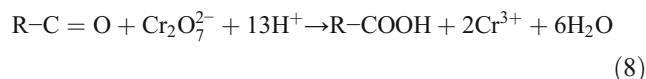
Cr(III)2p_{3/2}, and Cr(VI)2p_{3/2}, respectively. This result indicated that Cr(VI) was adsorbed by EPGA and partially reduced to Cr(III). Furthermore, we can conclude that 45.2% of the Cr(VI) anions have been reduced to Cr(III), from the calculations of peak area percentage.

Figure 9 c and d present the C1s and N1s core-level spectra of EPGA before and after Cr adsorption. The parameters of C1s and N1s peaks are shown in Table S2. From the C1s spectra before Cr adsorption, there are three component peaks, including C in graphite (284.6 eV), C–OH/C–N (285.9 eV) and C=O (288.5 eV). Cr adsorption slightly shifts the characteristic peaks of specific groups and the molar ratio of C=O decreases from 16.14 to 13.16%, which suggests that the C=O groups play an important role in the reduction process (Deng et al. 2017). For the N1s spectra, it consists of three parts—399.6 eV (=N–), 400.0 eV (pyrrolic-N), and 402.2 eV (pyrrolic-N-oxide). Compared with the N1s spectra before Cr adsorption, the molar ratio of pyrrolic-N decreased from 44.75 to 38.64% and pyrrolic-N-oxide decreased from 30.78 to 19.95% in the N1s spectra after Cr adsorption. While the

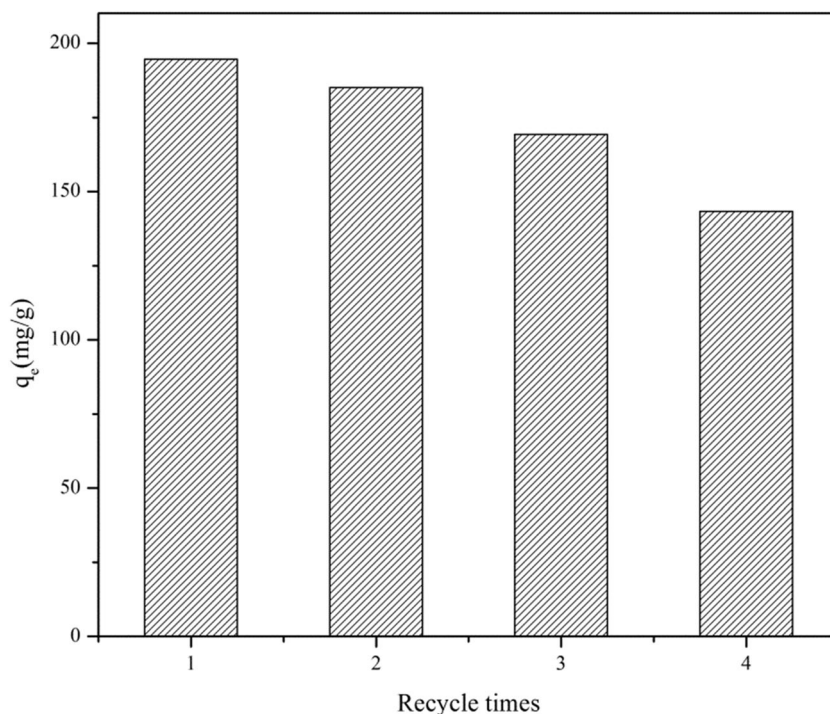
molar ratio of =N– increased from 24.47 to 41.40%. This result can be explained as follow: during the Cr removal process, Ppy is oxidized and pyrrolic-N and pyrrolic-N-oxide are converted to =N– groups (Fang et al. 2018). Therefore, it can be reasonably assumed that Cr(VI) is reduced to Cr(III) by the following equations:



or



On the basis of above reduction process, electrostatic attraction, ion exchange and chelation also involved in the adsorption process (Fig. 10). From the zeta potential (ζ) analysis, we know that the surface charge of EPGA is positive at low

Fig. 8 Reusability of EPGA

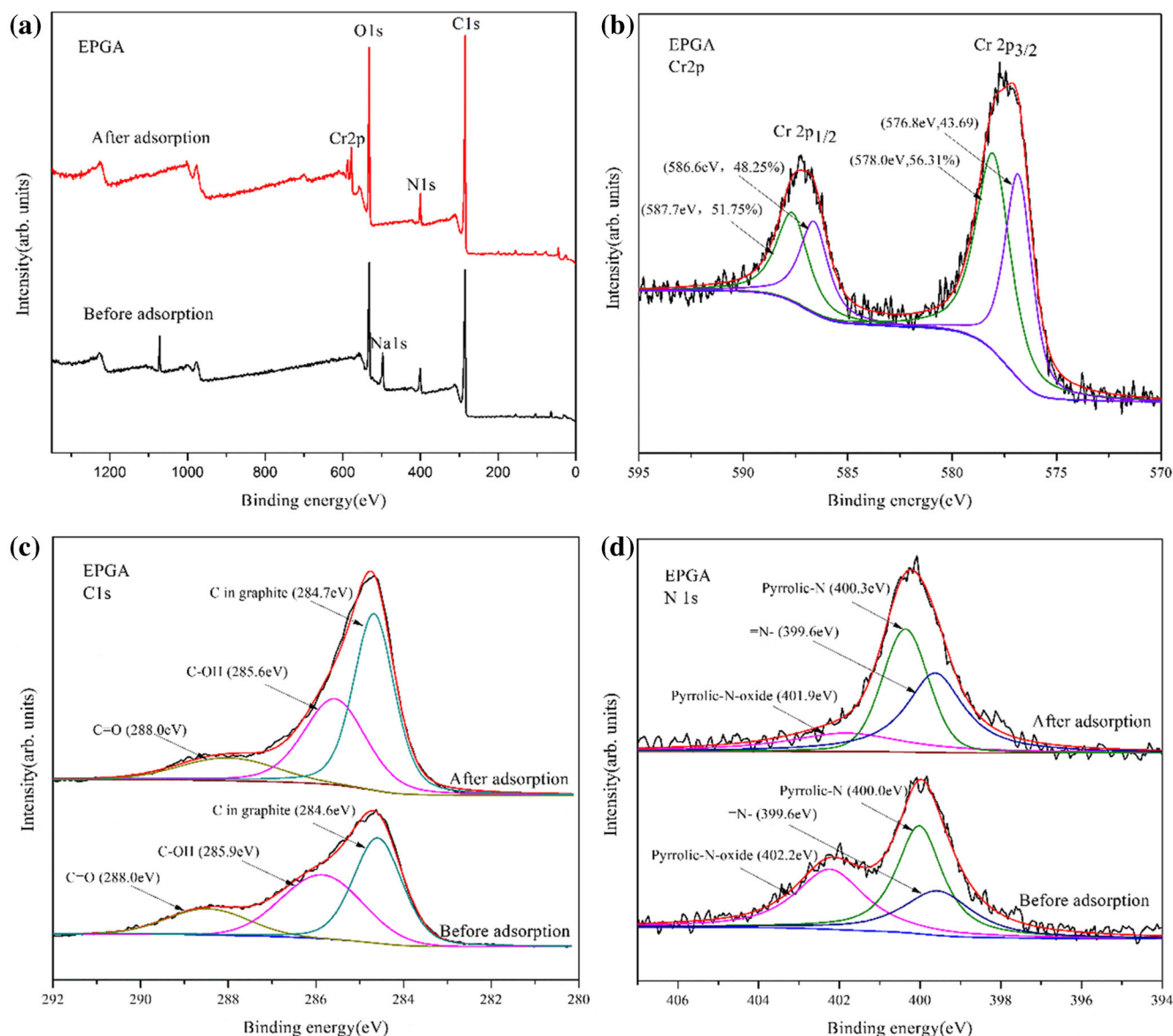
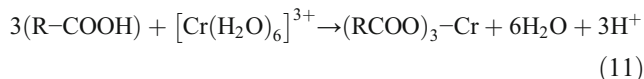
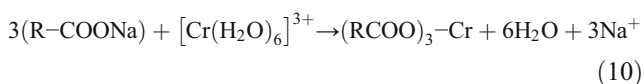


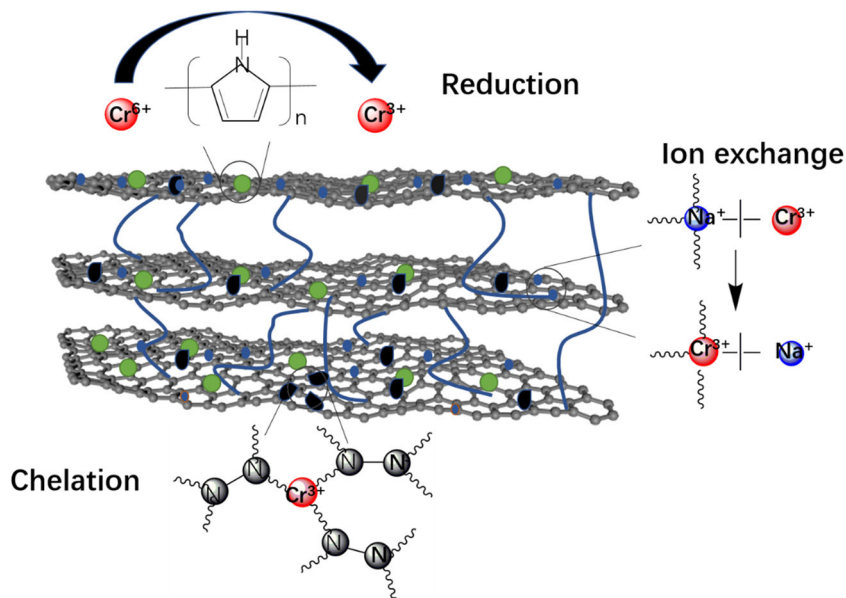
Fig. 9 XPS spectra of the EPGA before and after adsorption. **a** Full-range XPS spectrum. **b** Cr2p core-level spectra. **c** C1s core-level spectra. **d** N1s core-level spectra

pH. Therefore, Cr(VI) anions (HCrO_4^- and $\text{Cr}_2\text{O}_7^{2-}$) were attracted by plenty amount of protonated reactive groups—($-\text{NH}^+$), imine groups ($-\text{N}^+$) and ($-\text{COOH}^+$). As for Cr(III), $[\text{Cr}(\text{H}_2\text{O})_6]^{3+}$ specie was the main Cr(III) ions in an acidic solution. It can be adsorbed by ion exchange with Na^+ ions. In Fig. 9a, we can see that the Na1s peak disappeared in the full-range XPS spectrum of EPGA after Cr(VI) adsorption which confirms the existence of ion exchange during the removal process. Besides, EDTA-2Na is a common complexing agent in chemistry, which can be easily chelated with Cr(III) cations (Cerar 2015). The ion exchange and chelation can be summarized by Eqs. (10) and (11).



In order to reveal the relationship between adsorption and reduction during Cr(VI) removal, the concentration of total Cr, Cr(VI), and Cr(III) in solution upon different adsorption times were studied, as shown in Fig. 11. At the first minute of adsorption, 7.3 mg/L of Cr(III) could be measured in solution, probably because adsorption and reduction were carried out simultaneously, rather than that Cr(VI) was reduced after adsorption onto the EPGA surface. In the initial stage, the reduction reaction carried out rapidly, resulting in the reduction of a large amount of Cr(VI) to Cr(III), which was partially released into the solution. As the reducing active sites decreased,

Fig. 10 Possible adsorption mechanism of Cr(VI) ions on EPGA aerogel



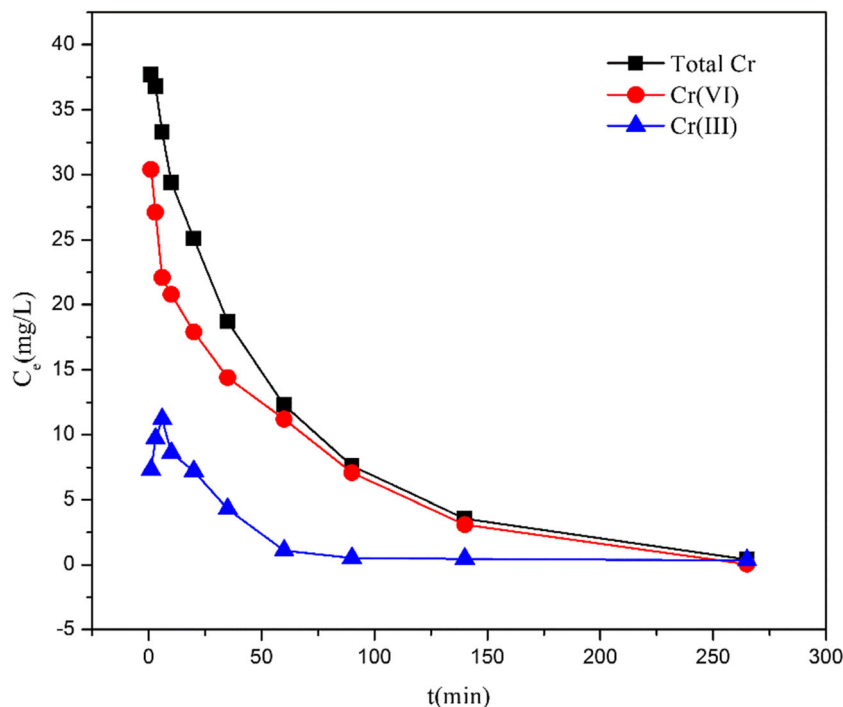
adsorption dominated at this stage. The concentration of Cr(III) in the solution gradually decreased until the adsorption equilibrium was reached.

Conclusions

A kind of functional rGO aerogel (EPGA) was synthesized successfully and used to remove Cr(VI) from aqueous solution. Experimental result indicated that the obtained EPGA

has an excellent adsorption ability for Cr(VI) anions, and the maximum adsorption capacity reached 361 mg/g at 298 K under pH of 2. In addition, when the initial concentration of Cr(VI) solution was below 50 mg/L, after adsorption by EPGA the concentration of Cr(VI) could reach the emission standard of Cr(VI) in industrial wastewater of China. The coexisting ions, including Cl^- , NO_3^- , SO_4^{2-} , PO_4^{3-} , Ni^+ , Cu^{2+} , Zn^{2+} , and Cd^{2+} , had no significant influence on removing Cr(VI), indicating that EPGA can selectively remove Cr(VI). The adsorption kinetic data fitted well with the

Fig. 11 Concentrations of total Cr, Cr(VI), and Cr(III) in solution upon different adsorption times on EPGA



pseudo-second-order kinetic model. The adsorption isotherm followed by the Freundlich isotherm and the adsorption process was endothermic. Moreover, EPGA had excellent regeneration ability and could repeat four adsorption-desorption cycles. In summary, EPGA is a potential candidate for efficient removal Cr(VI) anions from industrial wastewater.

Funding information This study is financially supported by the Social Development Fund of Guangdong Province (No. 2017A020216018) and Guangzhou Science and Technology Project (No. 201904010319).

References

- Aoudj S, Khelifa A, Drouiche N, Belkada R, Miroud D (2015) Simultaneous removal of chromium(VI) and fluoride by electrocoagulation–electroflotation: application of a hybrid Fe-Al anode. *Chem Eng J* 267:153–162. <https://doi.org/10.1016/j.cej.2014.12.081>
- Bhaumik M, Maity A, Srinivasu VV, Onyango MS (2011) Enhanced removal of Cr(VI) from aqueous solution using polypyrrole/Fe₃O₄ magnetic nanocomposite. *J Hazard Mater* 190:381–390. <https://doi.org/10.1016/j.jhazmat.2011.03.062>
- Cai W et al (2019) Preparation of thiourea-modified magnetic chitosan composite with efficient removal efficiency for Cr(VI). *Chem Eng Res Des* 144:150–158. <https://doi.org/10.1016/j.cherd.2019.01.031>
- Cao X, Yin Z, Zhang H (2014) Three-dimensional graphene materials: preparation, structures and application in supercapacitors. *Energy Environ Sci* 7:1850–1865. <https://doi.org/10.1039/c4ee00050a>
- Cerar J (2015) Reaction between chromium(III) and EDTA ions: an overlooked mechanism of case study reaction of chemical kinetics. *Acta Chim Slov*:538–545. <https://doi.org/10.17344/acsi.2015.1492>
- Cháuque EFC, Dlamini LN, Adelodun AA, Greyling CJ, Catherine Ngila J (2016) Modification of electrospun polyacrylonitrile nanofibers with EDTA for the removal of Cd and Cr ions from water effluents. *Appl Surf Sci* 369:19–28. <https://doi.org/10.1016/j.apsusc.2016.02.018>
- Chen JH et al (2015) Highly effective removal of Cu(II) by triethylenetetramine-magnetic reduced graphene oxide composite. *Appl Surf Sci* 356:355–363. <https://doi.org/10.1016/j.apsusc.2015.08.076>
- Chen L et al (2017) High performance agar/graphene oxide composite aerogel for methylene blue removal. *Carbohydr Polym* 155:345–353. <https://doi.org/10.1016/j.carbpol.2016.08.047>
- Cui L, Wang Y, Gao L, Hu L, Yan L, Wei Q, Du B (2015) EDTA functionalized magnetic graphene oxide for removal of Pb(II), Hg(II) and Cu(II) in water treatment: adsorption mechanism and separation property. *Chem Eng J* 281:1–10. <https://doi.org/10.1016/j.cej.2015.06.043>
- Deng L, Shi Z, Wang L, Zhou S (2017) Fabrication of a novel NiFe₂O₄/Zn-Al layered double hydroxide intercalated with EDTA composite and its adsorption behavior for Cr(VI) from aqueous solution. *J Phys Chem Solids* 104:79–90. <https://doi.org/10.1016/j.jpcs.2016.12.030>
- Ding CC, Cheng WC, Nie XQ, Yi FC (2017) Synergistic mechanism of U(VI) sequestration by magnetite-graphene oxide composites: evidence from spectroscopic and theoretical calculation. *Chem Eng J* 324:113–121
- Fang J, Gu ZM, Gang DC, Liu CX, Ilton ES, Deng BL (2007) Cr(VI) removal from aqueous solution by activated carbon coated with quaternized poly(4-vinylpyridine). *Environ Sci Technol* 41:4748–4753. <https://doi.org/10.1021/es061969b>
- Fang W, Jiang X, Luo H, Geng J (2018) Synthesis of graphene/SiO₂@polypyrrole nanocomposites and their application for Cr(VI) removal in aqueous solution. *Chemosphere* 197:594–602. <https://doi.org/10.1016/j.chemosphere.2017.12.163>
- Foo KY, Hameed BH (2010) Insights into the modeling of adsorption isotherm systems. *Chem Eng J* 156:2–10. <https://doi.org/10.1016/j.cej.2009.09.013>
- Geng J, Yin Y, Liang Q, Zhu Z, Luo H (2019) Polyethyleneimine cross-linked graphene oxide for removing hazardous hexavalent chromium: adsorption performance and mechanism. *Chem Eng J* 361:1497–1510. <https://doi.org/10.1016/j.cej.2018.10.141>
- Gong K et al (2018) Ultrasonic pretreated sludge derived stable magnetic active carbon for Cr(VI) removal from wastewater. *ACS Sustain Chem Eng* 6:7283–7291. <https://doi.org/10.1021/acssuschemeng.7b04421>
- Han L et al (2019) Carbon Dot–SnS₂ heterojunction photocatalyst for photoreduction of Cr(VI) under visible light: a combined experimental and first-principles DFT study. *J Phys Chem C* 123:2398–2409. <https://doi.org/10.1021/acs.jpcc.8b10059>
- Han Y, Cao X, Ouyang X, Sohi SP, Chen J (2016) Adsorption kinetics of magnetic biochar derived from peanut hull on removal of Cr(VI) from aqueous solution: Effects of production conditions and particle size. *Chemosphere* 145:336–341. <https://doi.org/10.1016/j.chemosphere.2015.11.050>
- He J, Chen JP (2014) A comprehensive review on biosorption of heavy metals by algal biomass: materials, performances, chemistry, and modeling simulation tools. *Bioresour Technol* 160:67–78. <https://doi.org/10.1016/j.biortech.2014.01.068>
- Huang YS, Li JX, Chen XP, Wang XK (2014) Applications of conjugated polymer based composites in wastewater purification. *RSC Adv* 4:62160–62178
- Jiang Y, Hu C, Cheng H, Li C, Xu T, Zhao Y, Shao H, Qu L (2016) Spontaneous, straightforward fabrication of partially reduced graphene oxide-polypyrrole composite films for versatile actuators. *ACS Nano* 10:4735–4741. <https://doi.org/10.1021/acsnano.6b01233>
- Jobby R, Jha P, Yadav AK, Desai N (2018) Biosorption and biotransformation of hexavalent chromium [Cr(VI)]: a comprehensive review. *Chemosphere* 207:255–266. <https://doi.org/10.1016/j.chemosphere.2018.05.050>
- Kera NH, Bhaumik M, Ballav N, Pillay K, Ray SS, Maity A (2016) Selective removal of Cr(VI) from aqueous solution by polypyrrole/2,5-diaminobenzene sulfonic acid composite. *J Colloid Interface Sci* 476:144–157. <https://doi.org/10.1016/j.jcis.2016.05.011>
- Khan ZU, Yan T, Shi L, Zhang D (2018) Improved capacitive deionization by using 3D intercalated graphene sheet–sphere nanocomposite architectures. *Environ Sci: Nano* 5:980–991. <https://doi.org/10.1039/c7en01246b>
- Li N, Yue Q, Gao B, Xu X, Kan Y, Zhao P (2018) Magnetic graphene oxide functionalized by poly dimethyl diallyl ammonium chloride for efficient removal of Cr(VI). *J Taiwan Inst Chem Eng* 91:499–506. <https://doi.org/10.1016/j.jtice.2018.05.028>
- Liang Q, Luo H, Geng J, Chen J (2018) Facile one-pot preparation of nitrogen-doped ultra-light graphene oxide aerogel and its prominent adsorption performance of Cr(VI). *Chem Eng J* 338:62–71. <https://doi.org/10.1016/j.cej.2017.12.145>
- Liu JT, Zhang WD, Ren ZQ, Ma JA (2009) The separation and concentration of Cr(VI) from acidic dilute solution using hollow fiber renewal liquid membrane. *Ind Eng Chem Res* 48:4500–4506. <https://doi.org/10.1021/ie8017669>
- Liu Y et al (2015) Preparation of a two-dimensional ion-imprinted polymer based on a graphene oxide/SiO₂ composite for the selective adsorption of nickel ions. *Langmuir* 31:8841–8851
- Lyu W et al (2019) Easy separated 3D hierarchical coral-like magnetic polyaniline adsorbent with enhanced performance in adsorption and

- reduction of Cr(VI) and immobilization of Cr(III). *Chem Eng J* 363: 107–119. <https://doi.org/10.1016/j.cej.2019.01.109>
- Mondal MK, Roy D, Chowdhury P (2018) Designed functionalization of reduced graphene oxide for sorption of Cr(VI) over a wide pH range: a theoretical and experimental perspective. *New J Chem* 42:16960–16971
- Ministry of Ecology and Environmental of the People's Republic of China, Water quality—Determination of chromium(VI)—1,5 Diphenylcarbazide spectrophotometric method (GB 7467–87)
- Ministry of Ecology and Environmental of the People's Republic of China, Water quality—Determination of total chromium—Potassium Permanganate Oxidation—Diphenylcarbazide Spectrophotometry method (GB 7466–87)
- Ministry of Ecology and Environmental of the People's Republic of China, Integrated wastewater discharge standard (GB 8978–96)
- Najafi F, Moradi O, Rajabi M, Asif M, Tyagi I, Agarwal S, Gupta VK (2015) Thermodynamics of the adsorption of nickel ions from aqueous phase using graphene oxide and glycine functionalized graphene oxide. *J Mol Liq* 208:106–113. <https://doi.org/10.1016/j.molliq.2015.04.033>
- Norouzi S et al (2018) Preparation, characterization and Cr(VI) adsorption evaluation of NaOH-activated carbon produced from Date Press Cake; an agro-industrial waste. *Bioresour Technol* 258:48–56. <https://doi.org/10.1016/j.biortech.2018.02.106>
- Shen C et al (2013) Highly efficient detoxification of Cr(VI) by chitosan-Fe(III) complex: process and mechanism studies. *J Hazard Mater* 244–245:689–697. <https://doi.org/10.1016/j.jhazmat.2012.10.061>
- Thao VD, Giang BL, Thu TV (2019) Free-standing polypyrrole/polyaniline composite film fabricated by interfacial polymerization at the vapor/liquid interface for enhanced hexavalent chromium adsorption. *RSC Adv* 9:5445–5452
- Tuo X et al (2018) Facile synthesis of magnetic polypyrrole composite nanofibers and their application in Cr(VI) removal. *Polym Compos* 39:1507–1513. <https://doi.org/10.1002/pc.24091>
- Upadhyay S, Saha AK, Sinha A (2019) High carbon iron filings (HCIF) and metal reducing bacteria (*Serratia* sp.) co-assisted Cr (VI) reduction: kinetics, mechanism and longevity. *J Environ Manag* 236:388–395. <https://doi.org/10.1016/j.jenvman.2019.02.015>
- Wan W, Zhang R, Li W, Liu H, Lin Y, Li L, Zhou Y (2016) Graphene-carbon nanotube aerogel as an ultra-light, compressible and recyclable highly efficient adsorbent for oil and dyes. *Environ Sci: Nano* 3: 107–113. <https://doi.org/10.1039/c5en00125k>
- Xu Y, Shi G, Duan X (2015) Self-assembled three-dimensional graphene macrostructures: synthesis and applications in supercapacitors. *Acc Chem Res* 48:1666–1675. <https://doi.org/10.1021/acs.accounts.5b00117>
- Yan Y, An Q, Xiao Z, Zheng W, Zhai S (2017) Flexible core-shell/bead-like alginate@PEI with exceptional adsorption capacity, recycling performance toward batch and column sorption of Cr(VI). *Chem Eng J* 313:475–486. <https://doi.org/10.1016/j.cej.2016.12.099>
- Zhang L, Luo H, Liu P, Fang W, Geng J (2016) A novel modified graphene oxide/chitosan composite used as an adsorbent for Cr(VI) in aqueous solutions. *Int J Biol Macromol* 87:586–596. <https://doi.org/10.1016/j.ijbiomac.2016.03.027>
- Zhang Y, Zhang D, Zhou L, Zhao Y, Chen J, Chen Z, Wang F (2018a) Polypyrrole/reduced graphene oxide aerogel particle electrodes for high-efficiency electro-catalytic synergistic removal of Cr(VI) and bisphenol A. *Chem Eng J* 336:690–700. <https://doi.org/10.1016/j.cej.2017.11.109>
- Zhang Z, Gao T, Si S, Liu Q, Wu Y, Zhou G (2018b) One-pot preparation of P(TA-TEPA)-PAM-RGO ternary composite for high efficient Cr(VI) removal from aqueous solution. *Chem Eng J* 343:207–216. <https://doi.org/10.1016/j.cej.2018.02.126>

Publisher's note Springer Nature remains neutral with regard to jurisdictional claims in published maps and institutional affiliations.